Research Article | Vol. 29, No. 10 / 10 May 2021 / Optics Express 14412

Optics EXPRESS

Dense-code free space transmission by local demultiplexing optical states of a composed vortex

B. PAROLI,* M. SIANO, AND M. A. C. POTENZA

Dipartimento di Fisica, Universitá degli Studi di Milano and INFN Sezione di Milano - via G. Celoria, 16, 20133 Milano, Italy
*bruno.paroli@unimi.it

Abstract: We describe an innovative data transmission scheme exploiting optical vortices to multiplex and demultiplex independent data channels in a standard asynchronous laser link. We report extensive results of the proof of concept of the method, successfully used to transmit two parallel ASCII strings, demultiplexed and decoded in the far field of the radiation beam. A phase locked two arms interferometer is proved to be effective even accessing a small portion of the beam only. Results prove the robustness and reliability of the method to perform dense-code free space transmissions over long distances even in presence of wavefront distortions. Applications and the extension to a larger number of parallel channels are discussed.

1. Introduction

Radiation with Orbital Angular Momentum (OAM) has been discovered [1–4] and formalized [5] at the end of the 20th century, proving that radiation with phase screw dislocations is solution of the Maxwell Equations. A number of experiments and applications have been conceived and performed in different fields of fundamental research and applied sciences: a few examples are in microscopy, to enhance the resolution limit [6,7]; in atomic physics, to increase the probability of non-dipolar transitions [8,9]; in astrophysics, to realize broadband coronagraphy [10–12], as well as to explore novel emission processes [13,14]. In all cases unprecedented results have been possible thanks to the vortex nature of radiation beams. A complementary area of interest deals with information, both in the classical [15–25] and quantum realms [26,27]. In both cases the main benefit stems from the additional degree of freedom introduced by the orbital angular momentum $L_z = hl/(2\pi)$, where l is an integer called topological charge and h is the Planck's constant. Contrarily to the two orthogonal polarization states, the number of possible orthogonal states of OAM radiation is not limited in principle, making it possible to realize dense–coding information also in a purely classical way by exploiting the helicity of the wavefront, which exhibits an azimuthal phase dependence $l\theta$ of the radiation field, where θ is the geometrical azimuthal angle.

Assessing the topological charge of OAM radiation requires to map the wavefront and extract the information about the genuine phase screw index, saying apart other phase changes such as curvature, aberrations, distortions, etc. This usually requires to detect a substantial portion of the beam section or the whole wavefront [28–31]. Moreover, as the distance increases, diffraction unavoidably imposes i) a global curvature and ii) increasing beam size. A receiver exploiting a substantial portion of the radiation wavefront will need to match the far field beam size, making the detection difficult or even impossible at arbitrarily large distances. Effectively recognizing OAM states by exploiting a small portion of the radiation beam will have obvious benefits in the field of telecommunications but also in all the applications where the entire wavefront is not accessible.

#417772 https://doi.org/10.1364/OE.417772
Journal © 2021 Received 16 Dec 2020; revised 8 Apr 2021; accepted 8 Apr 2021; published 28 Apr 2021

Optics EXPRESS

In [32,33] we have shown the effective feasibility of local measurements of the topological charge of OAM radiation. Nevertheless, the method adopted is ultimately inapplicable to telecommunications simply because of the need of multi–shot measurements.

In this work we explore a novel differential detection method that exploits local interferometry to distinguish different overlapped OAM states by accessing a small portion of the radiation wavefront only. A constant reference beam guarantees a precise monitoring of the spurious phase distortions. This combination successfully overcomes the limits discussed above, paving the way to a completely new approach for high dense data transmission. Moreover, the detection region does not need to include the OAM singularity and, depending on the instrument sensibility, the baseline needed to perform the local detection can be arbitrarily reduced, thus making the method very flexible. Finally, the number of overlapped states can be arbitrarily extended.

A multiplexed standard asynchronous laser link has been effectively realized in our laboratory. The link has been established between a transmission unit that modulates, multiplexes and shapes the composite vortex beam, and a receiver detecting a small fraction of the diffracted wavefront in the far field of the beam. A dense-code transmission has been realized by overlapping two simultaneous channels. An active feedback has been introduced to compensate the pointing instabilities and the wavefront perturbations specifically introduced by forcing air turbulence, through thermal instabilities. It is caused by free convection generated by imposing a temperature gradient. For the sake of simplicity this proof of principle has been done with two data strings transmitted in parallel at 1.2 kb/s. No loss of generality is introduced with this choice: faster transmission rates with arbitrary bandwidth can be similarly realized, provided that a balanced interferometer is adopted.

We stress that despite OAM transmissions of hundreds of Gb/s have been recently reported [34,35], the advantage we explore in this work is focused on achieving dense coding by using local detection. The proposed method has been verified at low transmission rate, however extension at higher transmission rates will be discussed for future developments.

2. Experimental setup

The composite beam is generated by overlapping a multiplexed, modulated He–Ne laser beam (λ = 632.8 nm) and a solid state laser (λ' = 635 nm) as the constant reference. The experimental setup to generate the OAM states and to match the curvatures of the two beams is schematically shown in Fig. 1.

Here a 10 mW He–Ne laser (λ = 632.8 nm) is modulated and multiplexed to encode the asynchronous data strings. The modulation exploits the On-Off Keying (OOK) technique, while two OAM states $l = 4$ and $l = -4$ are multiplexed. This is obtained by diffraction of the collimated, spatially filtered beam impinging onto specific CGHs realized through the SLM, constituted by a commercial Digital Micromirror Device (DMD). DMD is a high definition (1920 x 1080 pixels) orthogonal micromirror array (0.65" array diagonal) with 7.6 μm pixel pitch. CGHs as described in [36] are adopted to impose proper phase modulation on the diffracted beams, the vortex index being proportional to the diffraction order. The method used in Ref. [36] exploits transmissive SLM while we use a reflective SLM, in both cases the holograms are binarized from a grey scale to black and white. Among the many beams diffracted in both directions, the first order is collected along the optical path, with a relevant loss of light power.

After modulation and multiplexing, the beam is overlapped to the reference through a beam splitter and the composite vortex is generated. The reference is obtained by spatially filtering and collimating a solid state laser (λ' = 635 nm). The two beams have almost the same curvature at the receiver. It has been realized by positioning the waists of the reference and modulated beams of the spatial filters at similar distances from the beam splitter. By focusing the composite beam through the positive lens ahead the interferometer we further reduce the waists distance d_w below 1 mm. Since the beam is measured at a distance $z_w \approx 575$ mm from the waists in the far field of

Optics EXPRESS

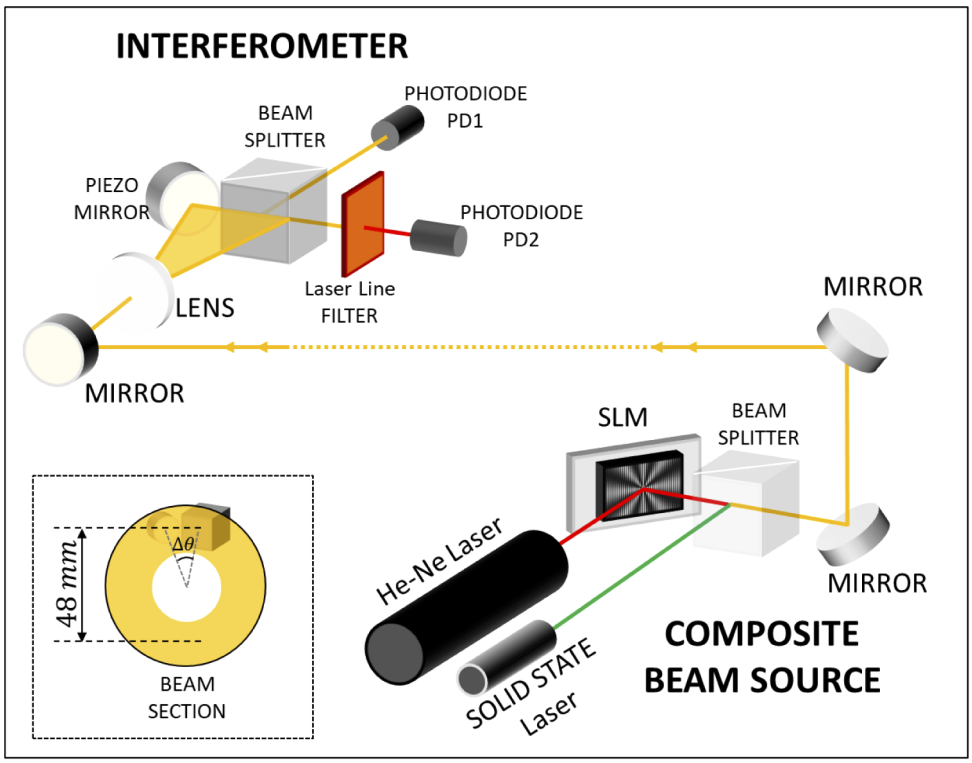

Fig. 1. Experimental setup. The composite beam is realized by overlapping a He–Ne laser (λ = 632.8 nm) (after modulation and multiplexing) and a solid state laser (λ' = 635 nm). The beam is expanded through a positive lens in such a way that the interferometer is illuminated by a small portion within an angular range $\Delta\theta \approx 30°$ (see inset). The interferometer is localized in the upper part of the beam, far from the singularity as shown in the inset.

both the reference and modulated beams we write $C_R \approx 1/z_w$ and $C_M \approx 1/(z_w + d_w)$, where C_M and C_R are the curvatures of the modulated and reference beam, respectively, thus the matching discrepancy is $(C_M - C_R)/C_R$<1%. The whole modulation and multiplexing system is mounted onto a stable granite optical bench.

The composite beam propagates a couple of meters far towards three mirrors and a focusing lens (focal length f = 60 mm), imposing a beam waist $w_0 \simeq 7$ μm at the focal plane. The detection system is placed in the far field, at a distance z = 575 mm from the beam waist corresponding to 2500 times the Rayleigh distance $z_R = \pi w_0^2/\lambda \simeq 0.23$ mm. The beam transversal size is ≈48 mm.

The detection, demultiplexing and decoding is finally performed by a two-arms compact interferometer composed by a piezo-mirror and a beam splitter fixed on a rigid metal slab (see Fig. 1). It is mounted on an independent, movable diagnostic unit remotely controlled. The piezo-mirror and the beam splitter axes are separated by 15 mm, both at approximately 25 mm from the vortex singularity. Being the beam size 48 mm in diameter, we collect a remarkable small portion of the transverse beam section only (see inset in Fig. 1).

The reference beam is exploited to lock the interferometer at the given phase ϕ_{lock}. The intensity of the interference pattern is detected by a silicon photodiode (PD1) and the corresponding photocurrent used as a feedback for locking the interferometer after a proper amplification. Since the reference beam intensity is about 100 times higher than the main beam intensity it prevails as reference signal to lock the interferometer. Moreover the intensity fluctuations of the main beam

Optics EXPRESS

during modulation are faster compared to the intensity variations due to pointing instability or air refractive index change and are filtered out by the feedback parameters. These conditions make the use of a laser line filter centered at 635 nm unnecessary.

A 1 nm bandwidth dichroic filter centered on the He–Ne laser line (632.8 nm) selects the signal–bearing light at the output of the interferometer after the beam splitter. The silicon photodiode (PD2) connected to a transimpedence amplifier reads the intensity level of the interferogram central fringe which directly depends on the adopted holograms used in transmission and codified as described here below.

3. String coding method

Information is multiplexed using OAM states with topological charges $l = 4$, $l = -4$ and modulated using the On-Off Keying (OOK) modulation. The binary information of the two OAM states gives origin to four possible combinations $(0, 0)$, $(0, 1)$, $(1, 0)$, $(1, 1)$ (D-bits), where the first and second bit of the pair are related to the OAM state $l = 4$, $l = -4$, respectively. Here the state "1" refers to "ON" while the state 0 refers to "OFF". Strings "UNIMI" and "O/A/M" are codified with standard ASCII codes. The asynchronous transmission (1.2 kb/s) has the format: 1

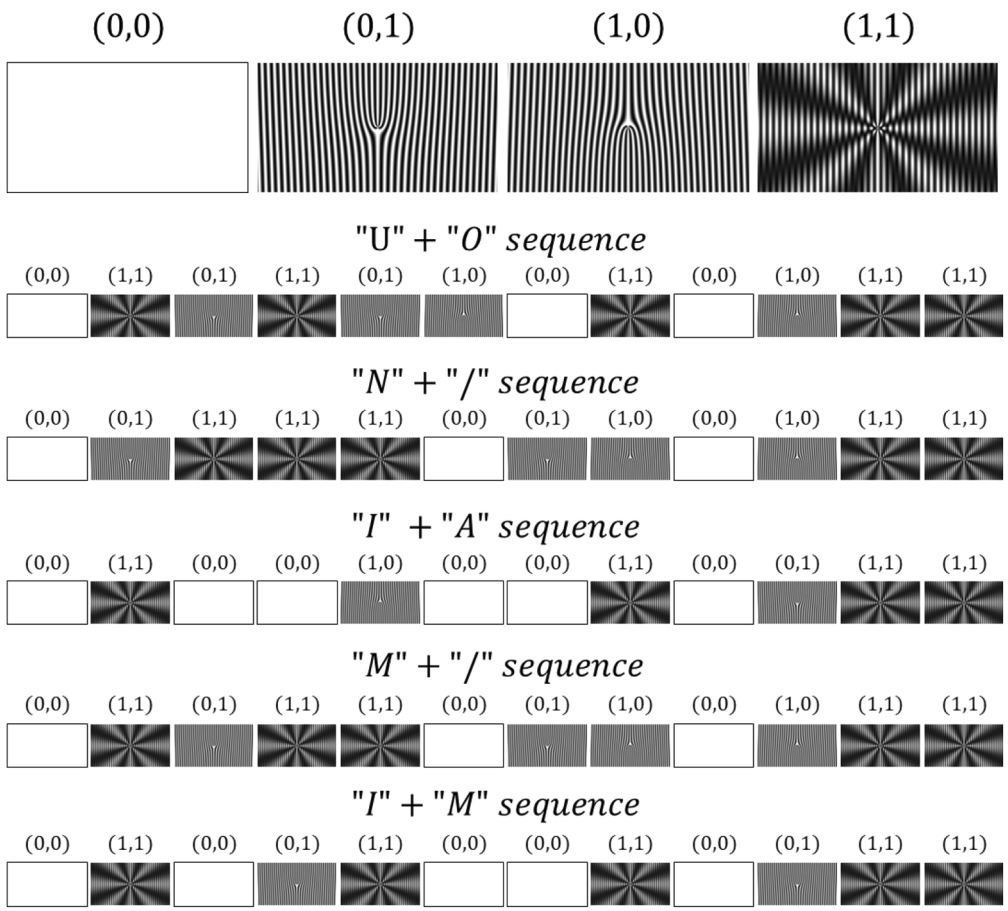

Fig. 2. Top. Holograms imposed on the SLM to codify the D-bit states $(0, 0)$, $(0, 1)$, $(1, 0)$, $(1, 1)$. Bottom. The complete sequence of the holograms to codify the overlapped strings "UNIMI" and "O/A/M" used in the asynchronous transmission.

Optics EXPRESS

bit star (LOW), 8 bit ASCII code, 1 bit parity (even parity), 2 bit stops (HIGH). The coding of the strings into the D-bit states are shown in Table 1. The number of D-bits for a pair of characters is 12, while the number of D-bits for a pair of strings (5 characters each) is 60. The four D-bit states are imposed on the radiation beam through the SLM, by using the computer generated holograms reported in Fig. 2 (top).

Table 1. String coding table. It is shown the bit-coding of each single character, the corresponding OAM states and the D-bit states. The "mix" state refers to the overlapping between the states with charges $l = 4$ and $l = -4$, while the "off" state corresponds to no transmitted light.

ASCII CODES	CHARACTERS	START	Bit 0	Bit 1	Bit 2	Bit 3	Bit 4	Bit 5	Bit 6	Bit 7	PARITY	STOP	STOP
55	**U**	0	1	0	1	0	1	0	1	0	1	1	1
4F	**O**	0	1	1	1	1	0	0	1	0	0	1	1
	OAM STATE	**OFF**	**MIX**	**−4**	**MIX**	**−4**	**+4**	**OFF**	**MIX**	**OFF**	**+4**	**MIX**	**MIX**
	D-BIT	(0,0)	(1,1)	(0,1)	(1,1)	(0,1)	(1,0)	(0,0)	(1,1)	(0,0)	(1,0)	(1,1)	(1,1)
4E	**N**	0	0	1	1	1	0	0	1	0	1	1	1
2F	**/**	0	1	1	1	1	0	1	0	0	0	1	1
	OAM STATE	**OFF**	**−4**	**MIX**	**MIX**	**MIX**	**OFF**	**−4**	**+4**	**OFF**	**+4**	**MIX**	**MIX**
	D-BIT	(0,0)	(0,1)	(1,1)	(1,1)	(1,1)	(0,0)	(0,1)	(1,0)	(0,0)	(1,0)	(1,1)	(1,1)
49	**I**	0	1	0	0	1	0	0	1	0	0	1	1
41	**A**	0	1	0	0	0	0	0	1	0	1	1	1
	OAM STATE	**OFF**	**MIX**	**OFF**	**OFF**	**+4**	**OFF**	**OFF**	**MIX**	**OFF**	**−4**	**MIX**	**MIX**
	D-BIT	(0,0)	(1,1)	(0,0)	(0,0)	(1,0)	(0,0)	(0,0)	(1,1)	(0,0)	(0,1)	(1,1)	(1,1)
4D	**M**	0	1	0	1	1	0	0	1	0	1	1	1
2F	**/**	0	1	1	1	1	0	1	0	0	0	1	1
	OAM STATE	**OFF**	**MIX**	**−4**	**MIX**	**MIX**	**OFF**	**−4**	**+4**	**OFF**	**+4**	**MIX**	**MIX**
	D-BIT	(0,0)	(1,1)	(0,1)	(1,1)	(1,1)	(0,0)	(0,1)	(1,0)	(0,0)	(1,0)	(1,1)	(1,1)
49	**I**	0	1	0	0	1	0	0	1	0	0	1	1
4D	**M**	0	1	0	1	1	0	0	1	0	1	1	1
	OAM STATE	**OFF**	**MIX**	**OFF**	**−4**	**MIX**	**OFF**	**OFF**	**MIX**	**OFF**	**−4**	**MIX**	**MIX**
	D-BIT	(0,0)	(1,1)	(0,0)	(0,1)	(1,1)	(0,0)	(0,0)	(1,1)	(0,0)	(0,1)	(1,1)	(1,1)

The (0,0) state is realized by setting all the micromirrors in such a way the light is deflected out of the transmission path. The (1,0) and (0,1) states are generated with digital holograms of the corresponding pure OAM states $l = 4$ and $l = -4$, respectively and computed as $H_{l=4} = |E_{m=4} + E_{m=0}|^2$, $H_{l=-4} = |E_{m=-4} + E_{m=0}|^2$, where m is the topological charge of the fields used in calculations, $E_{m=4} = \exp(i4\theta)$ and $E_{m=-4} = \exp(-i4\theta)$ are the complex fields of the OAM states depending on the azimuthal phase θ measured on a plane transverse to the propagation axis and $E_{m=0}$ is the complex field of a tilted plane wave (not collinear to $E_{m=4}$ and $E_{m=-4}$) that acts as a reference field to compute the holograms. The (1,1) state is generated with the hologram of the overlapped states computed as $H_{mix} = |E_{m=4} + E_{m=-4} + E_{m=0}|^2$, where $E_{m=4}$ and $E_{m=-4}$ are collinear, while $E_{m=0}$ is not collinear to $E_{m=4}$ and $E_{m=-4}$. The sequence of the states (as reported in Table 1) is temporized by using the internal clock of the DMD control board. The exposure time of the each hologram is 833 μs. In Fig. 2 (bottom) the complete sequence of holograms used to codify the overlapped strings "UNIMI" and "O/A/M" is shown.

Optics EXPRESS

4. Results and discussion

The 4-states of the modulated, composed beam with two OAM states ($l = 4$, $l = -4$) are converted by the interferometer in four corresponding intensity levels (see Eq. (2) below).

The intensity levels, as shown in Fig. 3, are measured with the photodiode PD2.

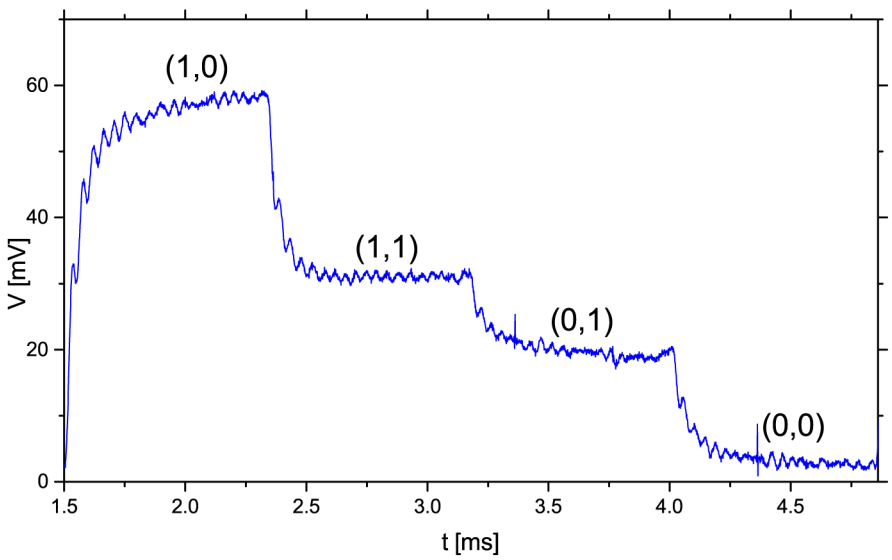

Fig. 3. Amplitude of the signal of the OAM states (0, 0), (0, 1), (1, 0), (1, 1), measured by the photodiode PD2.

The phase difference ΔP of the modulated radiation field at the input ports of the interferometer is proportional to the orbital angular momentum $L_z = \frac{hl}{2\pi}$ (see [32]) as

$$\Delta P \propto \left[\frac{2\pi L_z}{h} - \frac{k}{k'} l_0\right] \Delta\theta + \frac{k\Delta R}{k'} + \Delta\phi \,, \tag{1}$$

that in terms of the average intensity on the photodiode PD2 reads as

$$<I>=2\sqrt{I_{P1} I_{P2}} \cos \Delta P + I_{P1} + I_{P2} \,, \tag{2}$$

where $k = 2\pi/\lambda$, $k' = 2\pi/\lambda'$, λ is the wavelength of modulated beam, λ' is the wavelength of the reference beam, $l_0 = 0$ is the topological charge of the reference beam, $\Delta\theta$ is the azimuthal angle between the piezo-mirror and the beam-splitter axes measured on a plane transverse to the propagation axis (as shown in Fig. 1); ΔR is the phase difference of the reference beam due to the incident wavefront tilt on the detection plane; $\Delta\phi$ is a constant phase depending on the optical path difference between the interferometer arms, I_{P1} and I_{P2} are the intensities of the modulated beam through the interferometer arms measured on the photodiode PD2. $\Delta R = \phi_{lock} + cost$ is locked at a constant value by using the reference beam and a moveable piezo-mirror to cancel out any arbitrary phase due to the wavefront tilt of the incident radiation on the detection plane. Here *cost* is a phase constant that can be freely set (by using the feedback parameters) to change the working point. The setpoint is regulated to fix the phase ϕ_{lock} of the reference beam and to increase the intensity separation of the levels corresponding to the OAM states.

A standard link 1.2 kb/s has been implemented to send strings codified with ASCII codes. The strings are been simultaneously transferred by overlapping the OAM states $l = 4$, $l = -4$. Transmission is realized with a sequence (frame) of holograms produced by the SLM. Each

Optics EXPRESS

hologram reproduces a pair of overlapped bits (D-bit) as reported in section 3 and each pair of overlapped characters is codified with the standard frame 1 D-Bit START, 8 D-Bit DATA, 1 D-Bit PARITY, 2 D-bit STOP.

The OAM states are converted in four intensity states by the interferometer, as discussed previously. The signals of the received strings are shown in Fig. 4. Here the four intensity states $(0, 0)$ = 4.5 mV (black line), $(0, 1)$ = 18 mV (green line), $(1, 0)$ = 62.5 mV (yellow line) and $(1, 1)$ = 31.5 mV (red line) are well separated and distinguishable, thus the transmitted strings "UNIMI" and "O/A/M" are effectively received as shown by the comparison between the transmitted an received codes in Table 2.

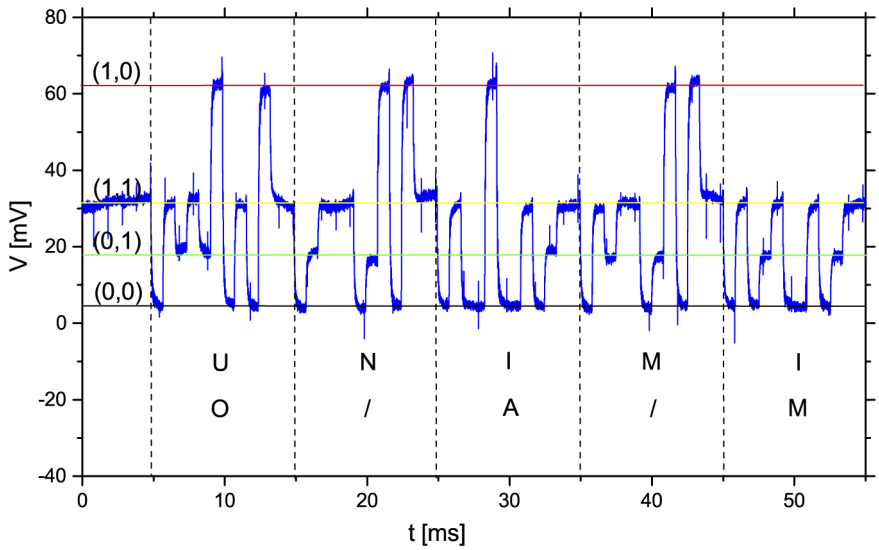

Fig. 4. Received signal of the asynchronous transmission at 1.2 kb/s affected by external perturbations as in Fig. 5. The signal distortions are suppressed by the reference beam. Signal is measured with the second photodiode PD2. The strings "UNIMI" and "O/A/M" have been transmitted simultaneously.

Table 2. Test table of the transmitted and received codes. The decoding process compares the amplitudes of the received signals (sampled at the D-bit center) with the fixed state levels (straight lines in Fig. 4). The received signals should be in the range $[V_{state} + \Delta V/2, V_{state} - \Delta V/2]$, where V_{state} is the corresponding fixed state level and ΔV the amplitude difference of the closest state.

STRINGS	Transmitted	Received	Parity error	Code error
U, O	55, 4F	55, 4F	none	none
N, /	4E, 2F	4E, 2F	none	none
I, A	49, 41	49, 41	none	none
M, /	4D, 2F	4D, 2F	none	none
I, M	49, 4D	49, 4D	none	none

The signal-to-noise ratio of the transmission is ≈ 7, where the signal is 6.75 mV, *i.e.* half of the amplitude differences of the closest states $[V_{(0,1)} - V_{(0,0)}]/2 = [V_{(1,1)} - V_{(0,1)}]/2$. Assuming that additive noise is the dominant cause of erroneous decisions, the corresponding Bit Error Rate (BER) is $<10^{-11}$. The BER has been evaluated as $erfc[(S/N)/\sqrt{2}]$.

Optics EXPRESS

4.1. Decoding in presence of beam pointing instabilities

The robustness against external disturbances has been verified by perturbing the position of the positive lens through an impulsive external force that acts on the lens mount, fixed on a bridge structure. This simply introduces pointing instabilities induced by mechanical vibrations. A periodic change of the wavefront tilt and position of the incident beam with respect to the plane of the interferometer input ports is introduced due to the structural resonances of the bridge. This effect is quantified by removing the reference beam and measuring the fluctuations of the photodiode signal during transmission. The results are shown in Fig. 5. The perturbation gives a modulation of the signals with oscillation period $\tau_p \approx 55$ ms, and 7 mV peak amplitude. This spurious modulation heavily affects the state decoding, the change being larger than half the state level difference. On the contrary, by exploiting the reference beam the spurious modulation is prevented, as shown in Fig. 4 and Table 2.

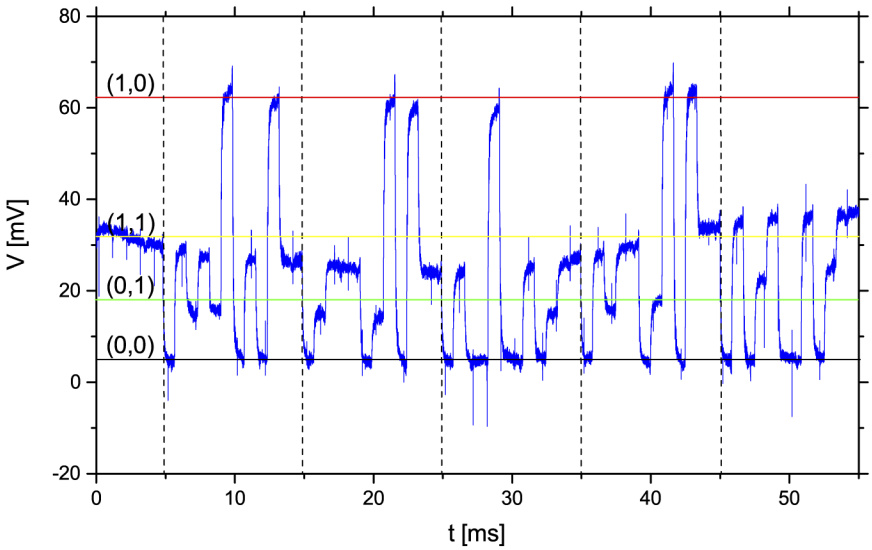

Fig. 5. Received signal of the asynchronous transmission at 1.2 kb/s corrupted by external perturbations (without the reference beam). Signal is measured with the photodiode PD2. The reference beam has been removed. Mechanical vibrations act as additional unwanted amplitude modulations.

4.2. Decoding signals perturbed by air turbulence

Transmission through the atmosphere will be heavily affected by air turbulence, introducing fluctuations of the air refractive index in space and time. We have stressed our link by imposing (quasi) stochastic wavefront distortions by means of air density fluctuations generated along the beam path by means of thermal free convection. A circular heater 155 mm in diameter is positioned 185 mm below the optical path of the composite beam in free propagation. The heater was then stabilized at a temperature of 70°C.

The effects of the refractive index changes are quantified by means of the mean-square-roots σ_V of the PD2 signal amplitude, in absence of the reference beam. Results obtained during time intervals one second long are shown in Fig. 6 as a function of the OAM states. They are compared to the same results obtained by introducing the reference beam. The corresponding S/N ratios are $S/N_{(1,0)} = 2.3$, $S/N_{(1,1)} = 1.1$, $S/N_{(0,1)} = 0.8$, $S/N_{(0,0)} = 6.2$, without the reference beam and $S/N_{(1,0)} = 5.7$, $S/N_{(1,1)} = 4.6$, $S/N_{(0,1)} = 4.6$, $S/N_{(0,0)} = 10.2$ with the reference beam.

Optics EXPRESS

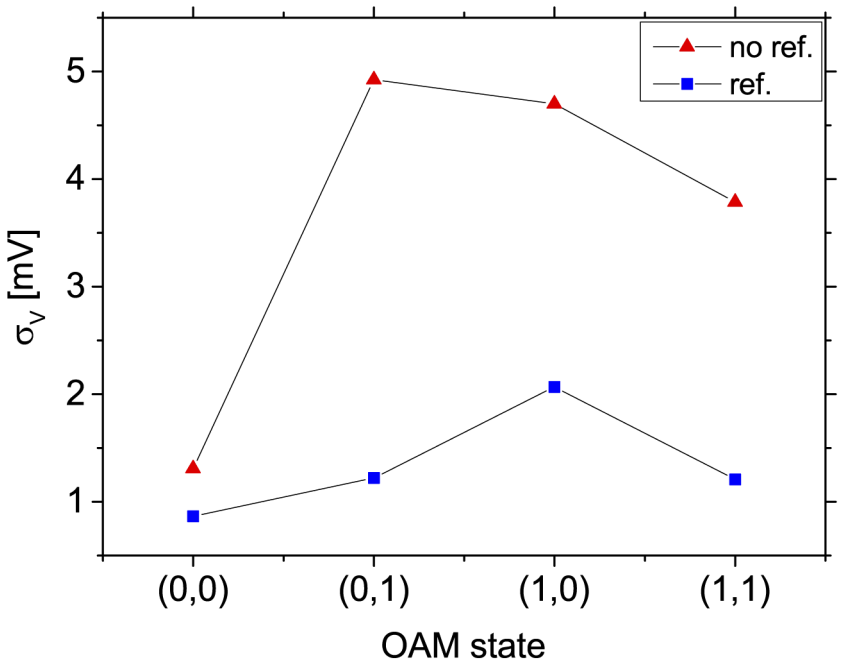

Fig. 6. Mean–square–root of the amplitude signal measured with the photodiode PD2 of the OAM states $(0,0)$, $(0,1)$, $(1,0)$, $(1,1)$, under wavefront perturbations induced by changes in the air refractive index forced by convection. Measurements are performed with the reference beam (blue squares) and without the reference beam (red triangles).

To evaluate the crosstalk of the states upon wavefront perturbation, a time sequence composed by the 4-states has been transmitted through the turbulent medium with and without the reference beam. The results are reported in Fig. 7 for single frame acquisition (single trace of the oscilloscope in a 60 ms time window) and in Fig. 8 for multi–frame acquisition (200 traces of the

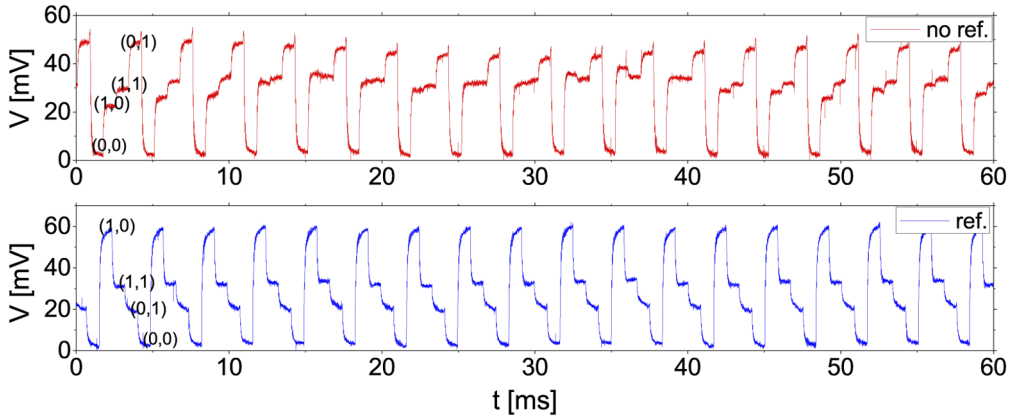

Fig. 7. Received signal of the OAM states $(0,0)$, $(0,1)$, $(1,0)$, $(1,1)$ measured with the photodiode PD2 under wavefront perturbations induced by changes in the air refractive index forced by convection. Measurements are performed without the reference beam (top) and with the reference beam (bottom).

Optics EXPRESS

oscilloscope each 50 ms long overlapped and visualized through the oscilloscope persistence map). Both cases show that OAM state levels are often overlapped and become indistinguishable in absence of the reference beam, making the transmission channel strongly unstable. On the contrary, the reference beam effectively prevents any overlapping.

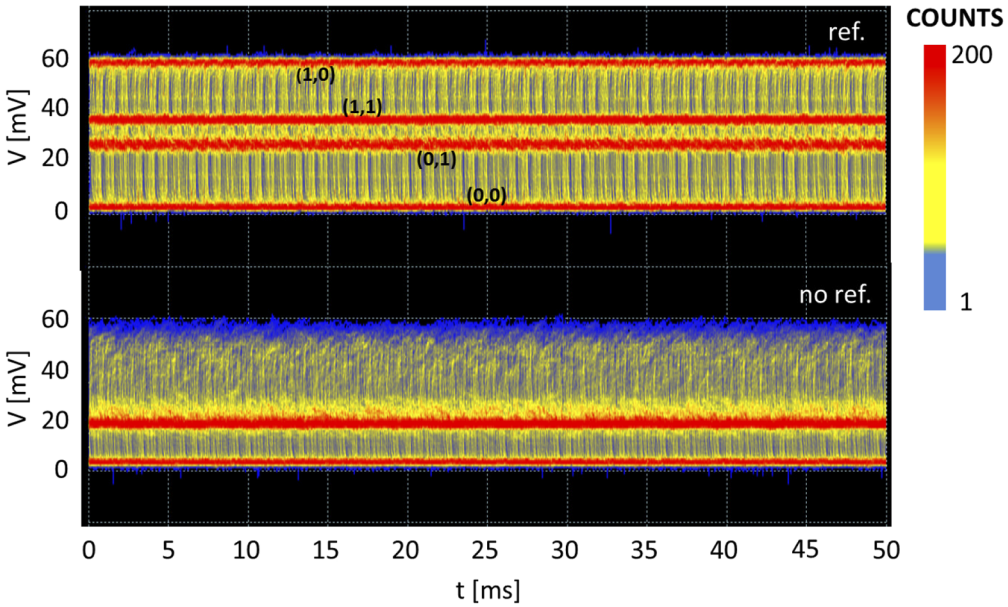

Fig. 8. Persistence map of the received signal measured with the photodiode PD2 of the OAM states $(0,0)$, $(0,1)$, $(1,0)$, $(1,1)$, under wavefront perturbations induced by changes in the air refractive index. Measurements are performed with the reference beam (up) and without the reference beam (bottom). The yellow regions are due to signal state transitions. The state levels in absence of the reference beam are overlapped and undistinguishable.

5. Conclusions

The differential method for the detection of the OAM radiation represents a unique strategy to overcome several standard issues in realizing long distance data transmission laser links. An optical transmission link based on a OOK modulation as a proof of concept of high density data transmission in free space propagation is effectively realized by using the composition of two beams in different frequency bands, matched in curvature. The standard asynchronous transmission with OAM multiplexing and demultiplexing has been implemented successfully with a BER $<10^{-11}$ (under stable air conditions).

Beam point instabilities, external vibrations, wavefront distortions induced by strong fluctuations in the air refractive index have been used to stress the link, providing the proof of a remarkable robustness. Indeed, since the wavefront perturbations are very similar in both the reference and main beams, the differential detection method effectively rejects the common mode phase changes. The method reveals a substantial improvement of the S/N ratios when compared to the single beam transmission, providing BERs of $2 \cdot 10^{-6}$ (with air convection) with the reference beam and $\approx 2 \cdot 10^{-1}$ without. The rejection is optimized since the wavelength difference is very small, $\lambda - \lambda' = 2.2$ nm.

Although relying on a laboratory mockup, the case of realistic laser beams obtained with conventional collimators and delivered over distances of tens of km is well reproduced in terms of power, size and interferometric detection of the composed wavefront. Of course, in the actual

Optics EXPRESS

case of ground based long–range transmission the propagation is critical, air turbulence and fog introduce wavefront distortions and spreads the OAM modes over a wide spectral range. This problem is completely prevented for in space communications. Nevertheless, pointing instabilities and relative motions between the receiver and transmitter pose important challenges for practical applications.

The local approach limits the efficiency and also the transmission distance, since only a small portion of the entire wavefront, and therefore power, is detected. For example, in our apparatus the received power (relative to the incident portion on the beam splitter and mirror) was 6% of the transmitted beam power (measurement performed with a photometer). By scaling the beam geometry, we find that with highly collimated beams with waist of, e.g., ten millimeters, at a distance of hundreds of km the beam size is a few meters. A receiver with a detection area of hundreds of cm^2 will collect a few percent of the transmitter power.

In this view the strictly local detection method plays a fundamental role in making the system independent of the wavefront tilt perturbations that are intrinsically compensated. The dependence of ΔP and $<I>$ on the azimuthal angle $\Delta\theta$ shown in Eq. (1) and Eq. (2) represents a much less critical issue: in fact the relative change of the $\Delta\theta$ implies a relative change of the same order for ΔP. For example, undesired displacement of the beam singularity due to pointing instabilities can occur but in this case to double erroneously the measured topological charge, the distance between the singularity and the interferometer should also double. This represents an unlikely condition. On the contrary, small inclinations between the wavefront and the detection plane generate large errors. In the current configuration an inclination between the wavefront and the detection plane of only 4 μ rad would produce an erroneous estimate of the topological charge by a factor of 2, without the reference beam compensation.

Extensions to devices operating more parallel channels and much higher bandwidths are possible with existing technologies. In our case, the transmission rate is currently limited by the used SLM to generate the holograms: it allows modulation and multiplexing by exploiting a single device but on the other hand limits the commutation frequency between the states. At Gb/s transmission faster modulation systems, e.g. electro-optical modulators, are necessary. In that case, the laser beam should be split in two paths, modulated separately and recombined after the spatial modulation of the OAM states. 10 mW output power lasers are compatible for kbit/s transmissions. For higher transmission bandwidths (GHz) the S/N of the receiver should be increased and lasers in the watt power range will be necessary. Another important factor that decreases the beam intensity reducing the S/N at the receiver is the power loss due to the spatial modulator. In the current setup this loss is very large due to the high number of diffraction orders generated by the micromirror array. The use of refractive elements such as spiral phase plates or sinusoidal holograms would be preferable.

Finally, the interferometer adopted in our proof of principle is characterized by two optical elements: the piezo-mirror and the beam splitter. This simple realization is less sensitive to external vibrations but the interferometer arms are unbalanced, limiting the maximum receiving band to $\approx$ 20 GHz in the current geometry. The interferometer will need to be balanced at hundreds GHz transmission rates. The receiver sensibility can be increased by increasing the distance between the piezo-mirror and the beam-splitter, the input phase difference ΔP being proportional to the azimuthal angle $\Delta\theta$. As it is evident, all these issues are related to limitations imposed by our laboratory realization. They can be overcome by conventional technologies pushing the data transfer rates up to the maximum. The proof of concept we provide here can therefore be adapted to work with conventional technologies to multiply the amount of transferred data.

It represents a breakthrough with respect to previous local measurements (see [32], since a rigorous single shot measurement is possible and proved to be effective enough to transfer data.

Acknowledgments. The authors acknowledge support from the University of Milan through the APC initiative.

Optics EXPRESS

Disclosures. The authors declare no conflicts of interest.

References

1. P. Coullet, L. Gil, and F. Rocca, "Optical vortices," Opt. Commun. **73**(5), 403–408 (1989).
2. M. Brambilla, L. A. Lugiato, V. Penna, F. Prati, C. Tamm, and C. O. Weiss, "Transverse laser patterns. II. Variational principle for pattern selection, spatial multistability, and laser hydrodynamics," Phys. Rev. A **43**(9), 5114–5120 (1991).
3. V. Yu. Bazhenov, M. V. Vasnetsov, and M. S. Soskin, "Laser beams with screw dislocations in the wavefronts," Pis'ma Zh. Eksp. Teor. Fiz. **52**, 1037–1039 (1990).
4. V. Yu. Bazhenov, M. S. Soskin, and M. V. Vasnetsov, "Screw dislocations in light wavefronts," J. Mod. Opt. **39**(5), 985–990 (1992).
5. L. Allen, M. W. Beijersbergen, R. J. C. Spreeuw, and J. P. Woerdman, "Orbital angular momentum of light and the transformation of Laguerre-Gaussian laser modes," Phys. Rev. A **45**(11), 8185–8189 (1992).
6. L. Yan, P. Gregg, E. Karimi, A. Rubano, L. Marrucci, R. Boyd, and S. Ramachandran, "Q-plate enabled spectrally diverse orbital-angular momentum conversion for stimulated emission depletion microscopy," Optica **2**(10), 900–903 (2015).
7. Ł. Płocinniczak, A. Popiołek-Masajada, J. Masajada, and M. Szatkowski, "Analytical model of the optical vortex microscope," Appl. Opt. **55**(12), B20–B27 (2016).
8. A. Picón, J. Mompart, J. R. de Aldana, L. Plaja, G. F. Calvo, and L. Roso, "Photoionization with orbital angular momentum beams," Opt. Express **18**(4), 3660 (2010).
9. R. Géneaux, A. Camper, T. Auguste, O. Gobert, J. Caillat, R. Taïeb, and T. Ruchon, "Synthesis and characterization of attosecond light vortices in the extreme ultraviolet," Nat. Commun. **7**(1), 12583 (2016).
10. G. A. Swartzlander Jr., E. L. Ford, R. S. Abdul-Malik, L. M. Close, M. A. Peters, D. M. Palacios, and D. W. Wilson, "Astronomical Demonstration of an Optical Vortex Coronagraph," Opt. Photonics News **19**(12), 22 (2008).
11. D. Mawet, "The vector vortex coronagraph: laboratory results and first light at Palomar observatory," Astrophys. J. **709**(1), 53–57 (2010).
12. E. Serabyn, C. M. Prada, P. Chen, and D. Mawet, "Vector vortex coronagraphy for exoplanet detection with spatially variant diffractive waveplates," J. Opt. Soc. Am. B **36**(5), D13–D19 (2019).
13. Y. Taira and M. Katoh, "Generation of Optical Vortices by Nonlinear Inverse Thomson Scattering at Arbitrary Angle Interactions," Astrophys. J. **860**(1), 45 (2018).
14. M. Katoh, "Optical vortex emitted from free electrons in nature," Proc. SPIE **11099**, 1109903 (2019).
15. J. Wang, J.-Y. Yang, I. M. Fazal, N. Ahmed, Y. Yan, H. Huang, Y. Ren, Y. Yue, S. Dolinar, M. Tur, and A. E. Willner, "Terabit free-space data transmission employing orbital angular momentum multiplexing," Nat. Photonics **6**(7), 488–496 (2012).
16. M. Krenn, R. Fickler, M. Fink, J. Handsteiner, M. Malik, T. Scheidl, R. Ursin, and A. Zeilinger, "Communication with spatially modulated light through turbulent air across Vienna," New J. Phys. **16**(11), 113028 (2014).
17. Z. Ghassemlooy, S. Zvanovec, M. Khalighi, W. O. Popoola, and J. Perez, "Optical wireless communication systems," Optik **151**, 1–6 (2017).
18. H. Chun, A. Gomez, C. Quintana, W. Zhang, G. Faulkner, and D. O'Brien, "A wide-area coverage 35Gb/s visible light communications link for indoor wireless applications," Sci. Rep. **9**(1), 4952 (2019).
19. A. Biswas, "NASA's Deep Space Optical Communications – an Update," in *Laser Congress 2019 (ASSL, LAC, LS&C)*, OSA Technical Digest (Optical Society of America, 2019), paper LTh1B.1.
20. Z. Wang, N. Zhang, and X.-C. Yuan, "High-volume optical vortex multiplexing and de-multiplexing for free-space optical communication," Opt. Express **19**(2), 482–492 (2011).
21. L. Li, R. Zhang, Z. Zhao, G. Xie, P. Liao, K. Pang, H. Song, C. Liu, Y. Ren, G. Labroille, P. Jian, D. Starodubov, B. Lynn, R. Bock, M. Tur, and A. E. Willner, "High-capacity free-space optical communications between a ground transmitter and a ground receiver via a UAV using multiplexing of multiple orbital-angular-momentum beams," Sci. Rep. **7**(1), 17427 (2017).
22. Y. Yan, G. Xie, M. P. J. Lavery, H. Huang, N. Ahmed, C. Bao, Y. Ren, Y. Cao, L. Li, Z. Zhao, A. F. Molisch, M. Tur, M. J. Padgett, and A. E. Willner, "High-capacity millimetre-wave communications with orbital angular momentum multiplexing," Nat. Commun. **5**(1), 4876 (2014).
23. J. Tan, Z. Zhao, Y. Wang, Z. Zhang, J. Liu, and N. Zhu, "12.5 Gb/s multi-channel broadcasting transmission for free-space optical communication based on the optical frequency comb module," Opt. Express **26**(2), 2099–2106 (2018).
24. W. C. Wang, H. Y. Wang, and G. R. Lin, "Ultrahigh-speed violet laser diode based free-space optical communication beyond 25 Gbit/s," Sci. Rep. **8**(1), 13142 (2018).
25. S. Sundbeck, I. Gruzberg, and D. G. Grier, "Structure and scaling of helical modes of light," Opt. Lett. **30**(5), 477–479 (2005).
26. A. Mair, A. Vaziri, G. Weihs, and A. Zeilinger, "Entanglement of the orbital angular momentum states of photons," Nature **412**(6844), 313–316 (2001).
27. M. Soskin, S. V. Boriskina, Y. Chong, M. R. Dennis, and A. Desyatnikov, "Singular optics and topological photonics," J. Opt. **19**(1), 010401 (2017).

Optics EXPRESS

28. J. Zhu, P. Zhang, D. Fu, D. Chen, R. Liu, Y. Zhou, H. Gao, and F. Li, "Probing the fractional topological charge of a vortex light beam by using dynamic angular double slits," Photonics Res. **4**(5), 187–190 (2016).
29. R. Chen, X. Zhang, Y. Zhou, H. Ming, A. Wang, and Q. Zhan, "Detecting the topological charge of optical vortex beams using a sectorial screen," Appl. Opt. **56**(16), 4868–4872 (2017).
30. G. Kulkarni, R. Sahu, O. S. Magana-Loaiza, R. W. Boyd, and A. K. Jha, "Single-shot measurement of the orbital-angular-momentum spectrum of light," Nat. Commun. **8**(1), 1054 (2017).
31. R. Aboushelbaya, K. Glize, A. F. Savin, M. Mayr, B. Spiers, R. Wang, N. Bourgeois, C. Spindloe, R. Bingham, and P. A. Norreys, "Measuring the orbital angular momentum of high-power laser pulses," Phys. Plasmas **27**(5), 053107 (2020).
32. B. Paroli, M. Siano, and M. A. C. Potenza, "A composite beam of radiation with orbital angular momentum allows effective local, single-shot measurement of topological charge," Opt. Commun. **459**, 125049 (2020).
33. B. Paroli, A. Cirella, I. Drebot, V. Petrillo, M. Siano, and M. A. C. Potenza, "Asymmetric lateral coherence of OAM radiation reveals topological charge and local curvature," J. Opt. **20**(7), 075605 (2018).
34. G. Xie, Y. Ren, Y. Yan, H. Huang, N. Ahmed, L. Li, Z. Zhao, C. Bao, M. Tur, S. Ashrafi, and A. E. Willner, "Experimental demonstration of a 200-Gbit/s free-space optical link by multiplexing Laguerre–Gaussian beams with different radial indices," Opt. Lett. **41**(15), 3447–3450 (2016).
35. N. Zhao, X. Li, G. Li, and J. M. Kahn, "Capacity limits of spatially multiplexed free-space communication," Nat. Photonics **9**(12), 822–826 (2015).
36. A. V. Carpentier, H. Michinel, and J. R. Salgueiro, "Making optical vortices with computer-generated holograms," Am. J. Phys. **76**(10), 916–921 (2008).